# Influence of Rare-Earth Variations on the Superconducting Properties of YBCO Films With and Without Artificial Pinning Centers

M. M. Aye, S. Mejia, H. Huhtinen, and P. Paturi

***Abstract*—Thin films of $Y_{1-x}Gd_xBa_2Cu_3O_{7-\delta}$ ($x = 0$, 1/3, 1/2, 2/3, 1), with and without $BaZrO_3$ (BZO) artificial pinning centers (APCs), were deposited by pulsed laser deposition (PLD) under growth parameters identical to those used for $YBa_2Cu_3O_{7-\delta}$. The effects of partial Gd substitution on the critical current density $J_c$ were systematically investigated and the results were found to differ between APC-free and BZO-doped films. Partial substitution of Y by Gd significantly enhanced $J_c$, particularly in films containing BZO nanorods. At 10 K, the $x = 2/3$ film with APC showed $J_c$ enhancements up to 45% over the $x = 0$ film across a wide magnetic field and temperature range. These findings strongly support Gd doping in YBCO as a highly promising route for future applications requiring maximized magnetic-field-dependent critical current densities.**

***Index Terms*—YGdBCO, pulsed laser deposition, critical current density, artificial pinning centers.**

## I. Introduction

AMONG high temperature superconductors (HTS), $YBa_2Cu_3O_{7-\delta}$ (YBCO) has long been the material of choice for coated conductors because of its excellent superconducting (SC) performance [1], [2], [3]. However, many studies have demonstrated that other $REBa_2Cu_3O_{7-\delta}$ (RE = rare earth element) thin films can provide distinct advantages over YBCO, including higher growth rates, smoother surfaces, and stronger flux pinning [4], [5], [6], [7]. Among the REBCO family, $GdBa_2Cu_3O_{7-\delta}$ (GdBCO) is one of the most widely investigated, as it combines a higher critical temperature $T_c$ with enhanced $J_c$ in high magnetic fields and a correspondingly higher irreversibility field $H_{irr}$ [8], [9], [10]. Furthermore, substituting $Y^{3+}$ with RE elements introduces variations in ionic size and chemical character, which influence defect structures, secondary phase formation, and strain fields. These modifications contribute directly to enhanced flux pinning and improved superconducting properties [11], [12], [13], [14].

Mixed systems such as YGdBCO have been proposed to take advantage of these effects [15], [16], [17], [18], [19], [20], [21], yet achieving the critical current density required for practical applications remains a challenge. In this work, we present a systematic study on the influence of various partial Gd substitutions in YBCO thin films grown by PLD under identical deposition conditions, both with and without artificial BZO pinning centers, to assess its impact on structural and superconducting performance.

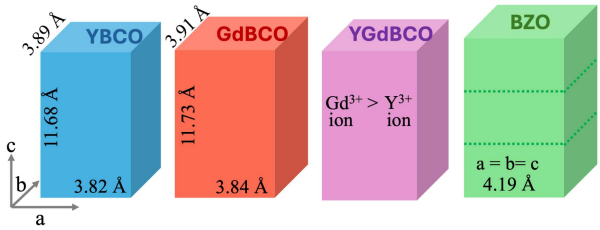


Fig. 1. Unit-cell–scale schematic illustrating lattice distortions in REBCO films induced by rare-earth substitution and BZO inclusion. Blue, red, and pink unit cells represent YBCO, GdBCO, and partially Gd-substituted YGdBCO, respectively, while green blocks represent three stacked BZO unit cells. In YGdBCO, random occupation of the rare-earth site by $Y^{3+}$ and $Gd^{3+}$ creates local lattice strain. Substitution of the larger $Gd^{3+}$ ion for $Y^{3+}$ leads to a modest expansion of the REBCO unit cell, whereas the larger cubic BZO lattice introduces additional misfit strain in REBCO–BZO containing films. Note that the unit cells are schematic and not drawn to scale.

## II. Experimental Details

Fig. 1 schematically shows how Gd substitution in YBCO leads to local variations in unit-cell dimensions, with further lattice strain generated by embedded BZO. In this study, $Y_{1-x}Gd_xBCO$ (APC-free) and $Y_{1-x}Gd_xBCO$:BZO (APC-film) thin films, with $x = 0$, 1/3, 1/2, 2/3, and 1, were deposited by PLD to investigate the effect of partial Gd substitution in YBCO with and without 4wt.%BZO (APCs). Targets with varying Gd concentrations were synthesized via the solid-state reaction method. All films were deposited on (100)-oriented $SrTiO_3$ (STO) substrates. The total thickness of films was ≈200 nm and identical deposition parameters were applied in all samples for comparison. A KrF excimer laser ($\lambda = 248$ nm) with 1.3 $Jcm^{-2}$ energy density and 5 Hz repetition rate was used. During the deposition, the substrate temperature was 750 °C, and the chamber pressure was 0.17 Torr. All films were *in situ* post-annealed in atmospheric pressure of $O_2$ for 10 min. More details on the PLD process are available in [22]. X-ray diffraction (XRD) (Philips Empyrean) was used for in-plane and out-of-plane analysis, while magnetic characterization was performed with a Quantum

Received 7 October 2025; revised 28 January 2026 and 16 February 2026; accepted 17 February 2026. Date of publication 23 February 2026; date of current version 5 March 2026. This work was supported by Jenny and Antti Wihuri Foundation. *(Corresponding author: M. M. Aye.)*

The authors are with the Wihuri Physical Laboratory, Department of Physics and Astronomy, University of Turku, FI- 20014 Turku, Finland (e-mail: moe.m.aye@utu.fi).

Color versions of one or more figures in this article are available at https://doi.org/10.1109/TASC.2026.3666832.

Digital Object Identifier 10.1109/TASC.2026.3666832

TABLE I
THE CRYSTALLOGRAPHIC PARAMETERS OF GD SUBSTITUTED YBCO APC-FREE AND APC-FILMS WITH VARYING GD CONTENTS, AS DETERMINED BY XRD MEASUREMENTS

| APC-free | $a$(Å) | $b$(Å) | $c$(Å) | $\Delta\theta(^\circ)$ | $V$(Å$^3$) | $\epsilon_{WH}$(%) | $r_c$(nm) |
|---|---|---|---|---|---|---|---|
| Gd0 | 3.838 | 3.859 | 11.660 | 0.096 | 172.7 | 0.075 | 12.2 |
| Gd1/3 | 3.851 | 3.873 | 11.658 | 0.080 | 173.9 | 0.066 | 15.6 |
| Gd1/2 | 3.856 | 3.879 | 11.659 | 0.079 | 174.4 | 0.060 | 15.7 |
| Gd2/3 | 3.856 | 3.890 | 11.660 | 0.076 | 174.9 | 0.054 | 16.1 |
| Gd1 | 3.857 | 3.903 | 11.657 | 0.074 | 175.5 | 0.048 | 16.1 |
| APC-film | | | | | | | |
| Gd0 | 3.848 | 3.873 | 11.710 | 0.090 | 174.5 | 0.226 | 9.3 |
| Gd1/3 | 3.851 | 3.895 | 11.708 | 0.094 | 175.6 | 0.100 | 15.2 |
| Gd1/2 | 3.858 | 3.889 | 11.707 | 0.089 | 175.7 | 0.089 | 16.2 |
| Gd2/3 | 3.861 | 3.895 | 11.706 | 0.087 | 176.1 | 0.075 | 17.2 |
| Gd1 | 3.864 | 3.896 | 11.709 | 0.094 | 176.3 | 0.084 | 16.5 |

Design Physical Property Measurement System (PPMS). $J_c$ was extracted from dc magnetization (up to 9 T, $H \parallel c$) at 10–77 K using the Bean model for rectangular films [23]. $T_c$ s were taken from the resistivity measurements and the angular dependence of $J_c$ was measured using the PPMS rotation stage, under fields of 0.5–8.0 T at 40 and 65 K.

## III. RESULTS AND DISCUSSION

### A. Improved Crystallinity by Gd Substitution in YBCO

X-ray diffraction study confirms that the films exhibit excellent $c$-axis orientation with no secondary phases. A prominent peak at $2\theta \approx 43.3^\circ$ in APC-films corresponds to the BZO (200) reflection, alongside strong YBCO (00l) peaks, confirming the epitaxial texture and phase purity of all deposited films. Additionally, no evidence of an $a$-axis oriented component was observed. The lattice constants $(a, b, c)$ and the relevant crystallographic parameters for all films are summarized in Table I. Detailed $\theta$–$2\theta$ scans of YBCO (005) (Fig. 2(a)) show reduced peak width $\Delta\theta$ upon Gd addition, indicating reduce pre-existing strain as YBCO and GdBCO unit cells adjust to nearly identical interplanar spacings, producing densely packed unit cells [24]. With further Gd substitution, peak narrowing suggests partial strain relief and more uniform d-spacing. The decline in Williamson-Hall microstrain $\epsilon_{WH}$ [25] with Gd content further implies that lattice mismatch stress between YBCO and GdBCO phases may be relieved by defect formation (e.g., stacking faults). The $c$ lattice parameters (Table I) show no significant change with Gd addition. In contrast, an increase in the $a$ and $b$ lattice parameters is evident, likely due to the lattice strain induced by the larger ionic radius of $Gd^{3+}$(1.053 Å) compared to $Y^{3+}$(1.019 Å) in eight-fold coordination, resulting in an increased cell volume with higher Gd content. This suggests that the strain primarily affects the $ab$-plane, with minimal impact on $c$ lattice parameter. The XRD patterns show no additional reflections or systematic peak shifts indicative of significant substitution of Zr or RE cations on unintended lattice sites. This is consistent with Zr forming a separate BZO phase, while RE-site mixing is accommodated within the lattice, with any local strain contributing primarily as peak broadening rather than distinct shifts.

XRD $\phi$-scans of YGdBCO (102) and $\omega$-scans of YGdBCO (005) in Fig. 2(b) show that both peak widths, $\Delta\phi$ and $\Delta\omega$, decrease with increasing Gd content in APC-films, reaching a minimum $\Delta\omega$ at Gd2/3 and a minimum $\Delta\phi$ at Gd1. In APC-free films, $\Delta\phi$ decreases from Gd0 to Gd1/3, remains approximately constant through Gd2/3, and decreases again at Gd1, whereas $\Delta\omega$ does not exhibit a clear trend and peaks at Gd0. Furthermore, the lattice coherence length $r_c$, derived from the (005) rocking curve width, systematically increases with Gd content (Table I). These results suggest that partial Gd substitution more effectively improves structural properties in APC-films, likely due to strain effects from accommodating three mismatched lattices (YBCO, GdBCO, and BZO) instead of two (YBCO and GdBCO) in APC-free films. Despite identical growth parameters, partial Gd substitution in YBCO films mitigates in-plane stress, reduces strain and number of defects, and improves epitaxial alignment, thereby enhancing crystallinity and interfacial coherence at YBCO/STO and YBCO/BZO/STO interfaces.

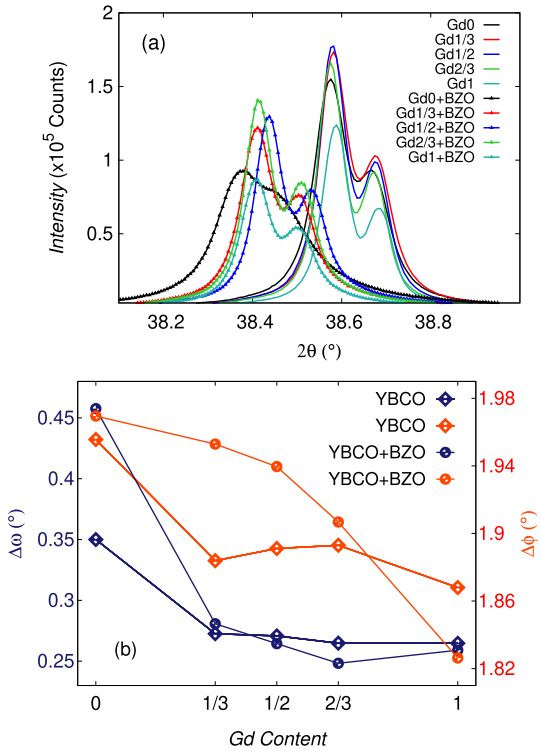


Fig. 2. (a) X-ray diffraction patterns of the (005) reflection of Gd-substituted YBCO films, including both APC-free and APC-containing samples and (b) the Gd content dependence of $\Delta\omega$ and $\Delta\phi$ for APC-free and APC-films.

### B. Improved SC Properties by Gd Substitution

The APC-free films show an onset $T_{c,onset}$ of $\approx 92$ K with only a slight increase in transition width $\Delta T_c$ as Gd content increased (Table II), when analyzed via resistive temperature dependencies. For the APC-films, $T_c$ increased with increasing Gd content up to Gd2/3 and then slightly decreased at Gd1. $\Delta T_c$ generally decreases with Gd substitution, although the Gd1 sample exhibits the widest transition. The smaller $\Delta T_c$ observed in partially Gd substituted APC-films can be attributed to improved crystalline quality, as evidenced by XRD results

TABLE II
ONSET CRITICAL TEMPERATURE ($T_c$) AND SUPERCONDUCTING TRANSITION WIDTH ($\Delta T_c$) OF APC-FREE AND APC-FILMS WITH VARYING GD CONTENT

| APC-free | Gd0 | Gd1/3 | Gd1/2 | Gd2/3 | Gd1 |
|---|---|---|---|---|---|
| $T_c$(K) | 91.5 | 91.3 | 91.6 | 91.4 | 91.9 |
| $\Delta T_c$ (K) | 1.29 | 1.34 | 1.36 | 1.43 | 1.74 |
| APC-film | | | | | |
| $T_c$(K) | 87.8 | 89.7 | 90.6 | 91.2 | 90.2 |
| $\Delta T_c$ (K) | 2.55 | 2.32 | 2.15 | 2.03 | 3.35 |

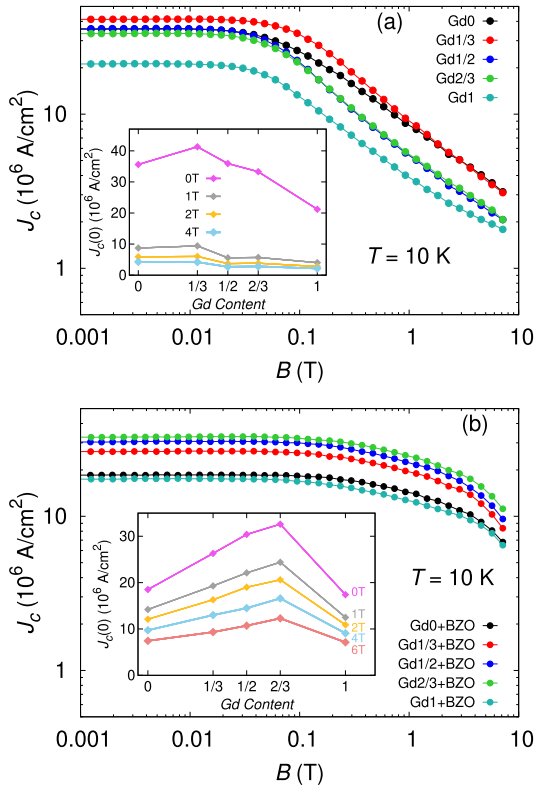


Fig. 3. The magnetic field dependence of $J_c$ measured at 10 K for (a) APC-free and (b) APC-films.

shown in Fig. 2(b) and Table I, which show narrower peak widths and a longer lattice coherence length ($r_c$).

Fig. 3(a) and (b) presents the $J_c - B$ characteristics of APC-free and APC-films under a magnetic field applied parallel to the $c$-axis at 10 K. As seen in Fig. 3(a), the $J_c(0)$ is only marginally affected by Gd substitution, with Gd1/3 displaying the largest improvement (16% over Gd0 at 10 K), while Gd1/2 and Gd2/3 show lower or comparable values for $J_c(0)$. At 0.05 T, both Gd1/2 and Gd2/3 exhibit reduced $J_c$ relative to Gd0, and Gd1/3 maintains only a slight improvement up to 0.1 T. However, $J_c$ in Gd1/3 decreases more rapidly in higher fields, eventually aligning with Gd0 above 0.1 T, indicating that enhancement in APC-free films is restricted to low fields, as clearly illustrated in the inset of Fig. 3(a).

In contrast, APC-films show significant benefit. As seen in Fig. 3(b), the most notable effect of Gd substitution is the improvement of self-field critical current density $J_c(0)$ in APC-films, when compared with $J_c(0)$ of Gd0 sample. At 10 K, $J_c(0)$ is enhanced by approximately 30%, 40%, and 45% for Gd1/3, Gd1/2, and Gd2/3, respectively, indicating a pronounced positive influence of Gd on crystalline quality, which also reflects the higher absolute $J_c$ across the entire magnetic field range. As seen in the inset figure of Fig. 3(b), Gd2/3 exhibits the highest $J_c$ in different magnetic fields.

The results highlight the contrasting effects of partial Gd substitution in APC-free and APC-films. In APC-free films, flux pinning originates from localized stress fields at YBCO/GdBCO interfaces, induced by the ionic radius mismatch between $Y^{3+}$ and $Gd^{3+}$ ions, which plays a primary role as observed in [26], [27]. This effect is supported by our XRD results, where variations in lattice parameters and unit-cell volume of Gd-substituted samples, compared with Gd0, indicate the generation of interfacial stress fields to accommodate lattice misfit. As the Gd content increases, however, the predominance of GdBCO domains reduces strain-field heterogeneity and diminishes defect density. Additionally, in RE-substituted films, the increased likelihood of cation exchange between $RE^{3+}$ and $Ba^{2+}$ can modify charge-carrier density and introduce further disorder in REBCO [14], [28], [29], [30]. Hence, the peak $J_c$ observed for Gd1/3 up to 0.1 T is attributed to Gd-induced strain, which adjusts oxygen content and charge distribution toward optimal doping [31]. Beyond this substitution level, the progressive weakening of strain fields, reduction in defect density, and modest decrease in electronic density due to diminished lattice distortion collectively lead to the observed decline in $J_c$.

In contrast, the role of Gd-induced strain in APC-films is more complex. The modified chemical environment and strain field at the growing film surface can influence the mobility of adatoms, thereby promoting the growth of the YBCO matrix and facilitating the incorporation of BZO. This may result in a higher density of effective pinning centers, although their detailed morphology and spatial distribution cannot be directly resolved in the present study. This interpretation is supported by our XRD results, which reveal enhanced in-plane and out-of-plane crystalline quality and longer lattice coherence lengths, implying reduced structural distortions, particularly at the BZO/YBCO interface where lattice mismatch typically induces strain. These improvements indicate higher overall crystallinity and improved connectivity between superconducting grains. Moreover, the influence of Gd/Ba substitution in APC-films appears to be limited, as it is expected to be largely confined to BZO-rich regions [18], [32]. In this context, correlated pinning centers associated with APC incorporation are likely to play a dominant role in flux pinning, while additional point-like and planar defects commonly reported in REBCO systems, such as stacking faults, local atomic disorder, and point defects associated with RE/Ba substitution may also contribute to the overall pinning landscape [7], [33]. Thus, in APC-films, the enhanced crystallinity together with the presence of effective pinning mechanisms inferred from transport measurements gives rise to an effective pinning landscape that significantly improves $J_c$. The highest $J_c$ observed for Gd2/3 is consistent with its higher $T_c$ and superior crystalline quality, as discussed earlier. Analysis of the $J_c(B)$ characteristics at various temperatures (not shown here) further shows that the qualitative behavior is similar across the entire temperature range up to 77 K, with Gd1/3 and Gd2/3 consistently exhibiting the highest $J_c(0)$ values in APC-free and APC-films, respectively. These

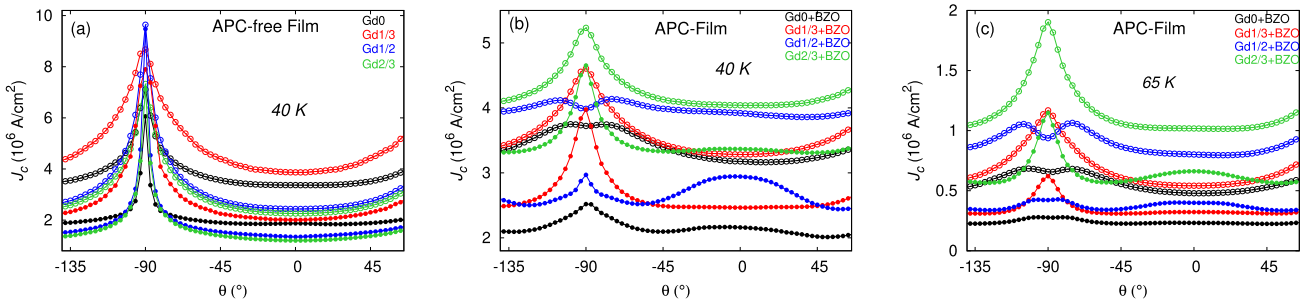


Fig. 4. Magnetic field angle dependence of $J_c$ at 1 T and 4 T for (a) APC-free films at 40 K, (b) APC-containing films at 40 K, and (c) APC-containing films at 65 K. Data at 1 T are shown as open circles, and data at 4 T as closed circles. The angles $\theta = -90^\circ$ and $0^\circ$ correspond to YBCO $ab$-plane and $c$-axis, respectively.

findings illustrate the balance between strain-related pinning effects and strain relaxation associated with Gd substitution in both APC-free and APC-films. In particular, Gd addition alleviates strain mismatch during BZO self-organization, leading to enhanced $J_c(0)$ relative to the YBCO and GdBCO compositions when Zr is incorporated, highlighting its beneficial effect on superconducting performance.

### C. Field Dependent Isotropy in $J_c$

Angular dependent $J_c$ measurements further elucidate the role of Gd substitution in YBCO films. As shown in Fig. 4(a) and (b), $J_c(\theta)$ behavior closely follows the trends observed in magnetic measurements with Gd1/3 showing the highest $J_c$ in APC-free films and Gd2/3 achieving the highest $J_c$ in APC-films, effects that are further enhanced at higher magnetic fields. In APC-free films, $J_c(\theta)$ at 1 T and 4 T (40 K) exhibits nearly isotropic behavior, with pronounced peaks at $\theta = -90^\circ$ ($B \parallel ab$-plane) that sharpen at higher fields (Fig. 4(a)). The consistent angular response across partially Gd-substituted samples suggests that comparable defect structures dominate the pinning landscape. At 1 T, the broad $ab$-plane peaks, together with the highest $J_c$, indicate that stacking faults and planar defects stabilize vortex alignment over an extended angular range [34]. At 4 T, the sharper $J_c$ peak at $B \parallel ab$-plane reflects strengthened intrinsic $ab$-plane pinning, highlighting the increasing contribution of correlated planar defects under higher magnetic fields. The angular dependence of the critical current density $J_c$ in APC-films is strongly influenced by both Gd substitution and temperature, reflecting the interplay between correlated and uncorrelated pinning. At 40 K and 1 T (Fig. 4(b)), none of the films exhibit a distinct $c$-axis peak, indicating that $c$-axis–correlated pinning is not dominant under these conditions. Gd0 and Gd1/2 show relatively isotropic behavior with dips near the $ab$-plane and pronounced shoulders, which are commonly attributed to variations in vortex step lengths at low vortex densities [35]. In contrast, Gd1/3 and Gd2/3 lack these shoulders and instead display pronounced $ab$-plane peaks, consistent with stronger intrinsic pinning. At 4 T, the angular response becomes more differentiated. Gd1/2 develops a clear $c$-axis peak, consistent with enhanced pinning by $c$-axis–aligned APCs [34], [36]. However, Gd1/3 and Gd2/3 exhibit much flatter angular dependences, despite Gd2/3 maintaining the highest absolute $J_c$. This demonstrates that a sharp $c$-axis peak is not a prerequisite for maximizing $J_c$, and that a more distributed pinning landscape can be more effective than a single dominant correlated pinning mechanism.

At the higher temperature of 65 K (Fig. 4(c)), the angular dependence of $J_c$ at 1 T follows a trend similar to that observed at 40 K and 1 T. However, at 4 T, the $c$-axis peak in Gd1/2 is significantly reduced, while Gd2/3 develops $c$-axis peak and continues to exhibit the highest overall $J_c$. This crossover suggests that the pinning mechanisms responsible for the low-temperature enhancement in Gd1/2 are more susceptible to thermal activation, whereas the pinning landscape in Gd2/3 remains effective over a wider temperature range. The non-monotonic angular $J_c$ behavior, particularly at intermediate Gd substitution, likely arises from enhanced strain heterogeneity and local disorder that preferentially strengthen low-temperature pinning but weaken at elevated temperatures. Notably, the absence of a sharp $c$-axis peak does not imply the absence of correlated pinning. While $c$-axis aligned BZO nanorods are highly effective correlated pinning centers, the coexistence of multiple pinning contributions such as nanorods, point defects, planar defects, and strain induced pinning can broaden or flatten the angular response. Hence, the consistently high $J_c$ observed in Gd2/3 across field orientations indicates a more balanced and effective pinning landscape resulting from the combined effects of Gd induced strain modification and BZO inclusion.

## IV. Conclusion

Partial Gd substitution in YBCO significantly enhances crystalline quality and superconducting performance, particularly improving $J_c(0)$. Strain fields induced by partial Gd substitution exert distinct influences on $J_c$ behavior in APC-free and BZO-doped YBCO films. While in APC-free films, the minor improvement in $J_c$ is only observed in 33% Gd-doped YBCO film and at magnetic fields below 0.1 T, APC-films with all Gd substitution concentrations exceed the Gd0 performance, with Gd2/3 providing the largest enhancement in $J_c$ of $\approx$45%. This highlights the critical role of both Gd substitution and its concentration in establishing the crystalline quality and effective flux pinning, particularly in YBCO films doped with artificial pinning centers such as BZO-nanorods. This study also provides a mechanistic understanding of Gd-induced microstructural evolution and pinning enhancement on STO substrates, offering a foundation for extending composition-engineered REBCO designs to technologically relevant coated-conductor substrates. In summary, our findings establish a systematic framework for co-optimizing rare-earth composition and artificial pinning strategies employed by HTS manufacturers to enhance REBCO conductor performance.

## REFERENCES


[1] T. G. Holesinger et al., "Progress in nanoengineered microstructures for tunable high-current, high-temperature superconducting wires," *Adv. Mater.*, vol. 20, pp. 391–407, 2008.

[2] S. R. Foltyn et al., "Materials science challenges for high-temperature superconducting wire," *Nature Mater.*, vol. 6, 2007, Art. no. 631.

[3] Y. Iijima and K. Matsumoto, "High-temperature-superconductor coated conductors: Technical progress in Japan," *Supercond. Sci. Technol.*, vol. 13, 2000, Art. no. 68.

[4] Y. Yoshida et al., "High-critical-current-density epitaxial films of $SmBa_2Cu_3O_{7-x}$ in high fields," *Jpn. J. Appl. Phys.*, vol. 44, pp. 129–132, 2005.

[5] C. Cai, B. Holzapfel, J. Hänisch, L. Fernández, and L. Schultz, "High critical current density its field dependence mixed rare earth (Nd,Eu,Gd,) BCO thin films," *Appl. Phys. Lett.*, vol. 84, 2004, Art. no. 377.

[6] S. H. Wee, A. Goyal, J. Li, Y. L. Zuev, S. Cook, and L. Heatherly, "The incorporation of nanoscale columnar defects comprised of self-assembled $BaZrO_3$ nanodots to improve the flux pinning and critical current density of $NdBa_2Cu_3O_{7-\delta}$ films grown on RABiTS," *Supercond. Sci. Technol.*, vol. 20, 2007, Art. no. 789.

[7] K. Takahashi et al., "Magnetic field dependence of $J_c$ for Gd-123 coated conductor on PLD-$CeO_2$ capped IBAD-GZO substrate tapes," *Supercond. Sci. Technol.*, vol. 18, 2005, Art. no. 1118.

[8] T. Iguchi, T. Araki, Y. Yamada, I. Hirabayashi, and H. Ikuta, "Fabrication of Gd-Ba-Cu-O films by the metal-organic deposition method using trifluoroacetates," *Supercond. Sci. Technol.*, vol. 15, 2002, Art. no. 1415.

[9] A. Kaneko et al., "Fabrication of $REBa_2Cu_3O_{7-y}$ film by advanced TFA-MOD process," *Physica C*, vol. 412–414, 2004, Art. no. 926.

[10] N. Haberkorn, F. Lovey, A. M. Condó, and J. Guimpel, "High-resolution transmission electron microscopy study of the interfaces and stacking defects in superconducting/magnetic perovskite superlattices," *J. Appl. Phys.*, vol. 97, 2005, Art. no. 053511.

[11] A. R. Devi, V. S. Bai, P. V. Patanjali, R. Pinto, N. H. Kumar, and S. K. Malik, "Enhanced critical current density due to flux pinning from lattice defects in pulsed laser ablated $Y_{1-x}Dy_x$BCO thin films," *Supercond. Sci. Technol.*, vol. 13, 2000, Art. no. 935.

[12] J. L. MacManus-Driscoll et al., "Systematic enhancement of in-field critical current density with rare-earth ion size variance on superconducting Rare-Earth barium cuprate films," *Appl. Phys. Lett.*, vol. 84, 2004, Art. no. 5329.

[13] J. L. MacManus-Driscoll et al., "Rare Earth ion size effects and enhanced critical current densities in $Y_{2/3}Sm_{1/3}Ba_2Cu_3O_{7-x}$ coated conductors," *Appl. Phys. Lett.*, vol. 86, 2005, Art. no. 032505.

[14] K. Miyachi, K. Sudoh, Y. Ichino, Y. Yoshida, and Y. Takai, "The effect of the substitution of Gd for Ba site on $Gd_{1+x}Ba_{2-x}Cu_3O_{6+\delta}$ thin films," *Physica C*, vol. 392–396, 2003, Art. no. 1261.

[15] M. Miura, M. Yoshizumi, T. Izumi, and Y. Shiohara, "Formation mechanism of $BaZrO_3$ nanoparticles in $Y_{1-x}Sm_xBa_2Cu_3O_y$-coated conductors derived from trifluoroacetate metal-organic deposition," *Supercond. Sci. Technol.*, vol. 23, 2010, Art. no. 014013.

[16] M. Miura et al., "Thermodynamic approach for enhancing superconducting critical current performance," *NPG Asia Mater.*, vol. 14, 2022, Art. no. 85.

[17] A. Kaneko et al., "Fabrication of $Y_{1-x}RE_xBa_2Cu_3O_{7-y}$ film by advanced TFA-MOD process," *Physica C*, vol. 426-431, 2005, Art. no. 949.

[18] V. Selvamanickam et al., "Effect of rare-earth composition on microstructure and pinning properties of Zr-doped (Gd, Y)$Ba_2Cu_3O_x$ superconducting tapes," *Supercond. Sci. Technol.*, vol. 25, 2012, Art. no. 045012.

[19] J. L. MacManus-Driscoll et al., "Guidelines for optimizing random and correlated pinning in rare-earth-based superconducting films," *Supercond. Sci. Technol.*, vol. 19, pp. S55–S59, 2006.

[20] J. MacManus-Driscoll and S. Wimbush, "Processing and application of high-temperature superconducting coated conductors," *Nature Rev. Mater.*, vol. 6, pp. 587–604, 2021.

[21] K. Tsuchiya et al., "Superconducting properties of commercial REBCO-coated conductors with artificial pinning centers," *Supercond. Sci. Technol.*, vol. 34, 2021, Art. no. 105005.

[22] M. Peurla et al., "Optimization of the $BaZrO_3$ concentration in YBCO films prepared by pulsed laser deposition," *Supercond. Sci. Technol.*, vol. 19, pp. 767–771, 2006.

[23] H. P. Wiesinger, F. M. Sauerzopf, and H. W. Weber, "On the calculation of $J_c$ from magnetization measurements on superconductors," *Physica C*, vol. 203, pp. 121–128, 1992.

[24] T. J. Haugan, T. A. Campbell, N. A. Pierce, M. F. Locke, I. Maartense, and P. N. Barnes, "Microstructural and superconducting properties of $Y_{1-x}Eu_xBa_2Cu_3O_{7-\delta}$ films: $x = 0$–1," *Supercond. Sci. Technol.*, vol. 21, 2008, Art. no. 025014.

[25] M. Birkholz, *Thin Film Analysis by X-Ray Scattering*. Hoboken, NJ, USA: Wiley-VCH, 2006.

[26] Y. Li et al., "Positron annihilation study the stress-field pinning mechanism in (Eu,Y)-123 superconductors," *Physica C*, vol. 314, pp. 55–68, 1999.

[27] H. H. Wen, Z. X. Zhao, R. L. Wang, H. C. Li, and B. Yin, "Evidence for the lattice-mismatch-stress-field induced flux pinning in $(Gd_{1-x}Y_x)Ba_2Cu_3O_{7-\delta}$ thin films," *Physica C*, vol. 262, pp. 81–88, 1996.

[28] L. Civale et al., "Angular-dependent vortex pinning mechanisms in $YBa_2Cu_3O_7$ coated conductors and thin films," *Appl. Phys. Lett.*, vol. 84, pp. 2121–2123, 2004.

[29] Q. X. Jia et al., "Comparative study of $REBa_2Cu_3O_7$ films for coated conductors," *IEEE Trans. Appl. Supercond.*, vol. 15, no. 2, pp. 2723–2726, Jun. 2005.

[30] S. Lee, K. Hirose, T. Yokoyama, N. Chikumoto, T. Kakeshita, and K. Nakao, "Study of compositional and artificial pinning effects on superconductivity of pulsed-laser deposited Gd-123 films for coated conductor applications," *IEEE Trans. Appl. Supercond.*, vol. 17, no. 2, pp. 3278–3281, Jun. 2007.

[31] A. Kinoshita et al., "Development of a thick GdBCO and $ZrO_2$-doped GdBCO film with a high critical current on a PLD-$CeO_2$/IBAD-GZO metal substrate," *Physica C*, vol. 463–465, 2007, Art. no. 630.

[32] G. Majkic et al., "New insight into strain and composition of $BaZrO_3$ nanorods in REBCO superconductor," *Supercond. Sci. Technol.*, vol. 34, 2021, Art. no. 115002.

[33] L. Civale et al., "Influence of crystalline texture on vortex pinning near the $ab$-plane in $YBa_2Cu_3O_7$ thin films and coated conductors," *Physica C*, vol. 412–414, pp. 976–982, 2004.

[34] B. Maiorov et al., "Synergetic combination of different types of defect to optimize pinning landscape using $BaZrO_3$-doped $YBa_2Cu_3O_7$," *Nature Mater.*, vol. 8, pp. 398–404, 2009.

[35] P. Paturi, "The vortex path model and angular dependence of $J_c$ in thin YBCO films deposited from undoped and $BaZrO_3$-doped targets," *Supercond. Sci. Technol.*, vol. 23, 2010, Art. no. 025030.

[36] F. J. Baca et al., "Interactive growth effects of rare-earth nanoparticles on nanorod formation in $YBa_2Cu_3O_x$ thin films," *Adv. Funct. Mater.*, vol. 23, pp. 4826–4831, 2013.